Heliyon 8 (2022) e10336

Contents lists available at ScienceDirect

Heliyon

journal homepage: www.cell.com/heliyon

Research article

Solvent-dependent activity of *Candida antarctica* lipase B and its correlation with a regioselective mono aza-Michael addition - experimental and molecular dynamics simulation studies

Zohreh Nazarian [a,b,*], Seyed Shahriar Arab [a]

[a] Faculty of Biological Sciences, Tarbiat Modares University, Jalal Highway, Tehran 14115-154, Iran
[b] Department of Chemistry and Petroleum Sciences, Shahid Beheshti University, Evin, Tehran 1983963113, Iran

GRAPHICAL ABSTRACT

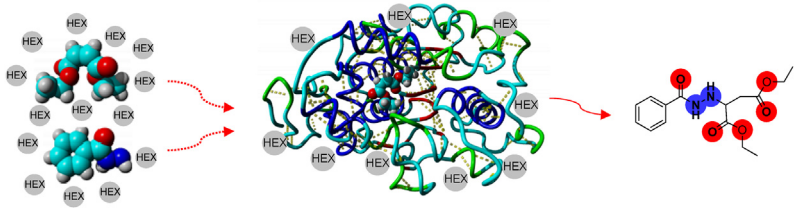

ARTICLE INFO

Keywords:
aza-Michael addition
Regioselective synthesis
CALB
Biocatalysis
Computational simulation
Molecular dynamics simulation

ABSTRACT

With the aim of gaining understanding of the molecular basis of commercially available *Candida antarctica* lipase B (CALB) immobilized on polyacrylic resin catalyzed regioselective mono aza-Michael addition of Benzhydrazide to Diethyl maleate we decided to carry out molecular dynamics (MD) simulation studies in parallel with our experimental study. We found a correlation between the activity of CALB and the choice of solvent. Our study showed that solvent affects the performance of the enzyme due to the binding of solvent molecules to the enzyme active site region, and the solvation energy of substrates in the different solvents. We also found that CALB is only active in nonpolar solvent (*i.e.* Hexane), and therefore we investigated the influence of Hexane on the catalytic activity of CALB for the reaction. The results of this study and related experimental validation from our studies have been discussed here.

1. Introduction

Lipases (triacylglycerol hydrolases E.C. 3.1. 1.3) are the most widely used versatile enzymes in organic synthesis, mainly because of its selectivity, commercial availability, broad specificity, and tolerance towards organic solvents, extreme temperature and pH (Angajala et al., 2016). The concept of "promiscuity" is considered as a useful phenomenon, which can expand the application of lipase as a biocatalyst (Dwivedee et al., 2018) leading to C–C bond and C-heteroatom (*e.g.* C–N, C–O, C–S coupling) bond construction, oxidative procedures, and unique hydrolytic reactions (Busto et al., 2010). Among all the hydrolases used in promiscuously catalysis, *Candida antarctica* lipase B known as CALB is one of the most widely used biocatalysts in industry. CALB is a serine hydrolase belonging to the folding family of α/β hydrolases it was firstly obtained from the *Candida antarctica* yeast, with the catalytic triad consists of Ser105,

* Corresponding author.
E-mail addresses: nazarianzohreh@yahoo.com.au, z_nazariyan@sbu.ac.ir (Z. Nazarian).

https://doi.org/10.1016/j.heliyon.2022.e10336
Received 13 March 2022; Received in revised form 21 May 2022; Accepted 12 August 2022

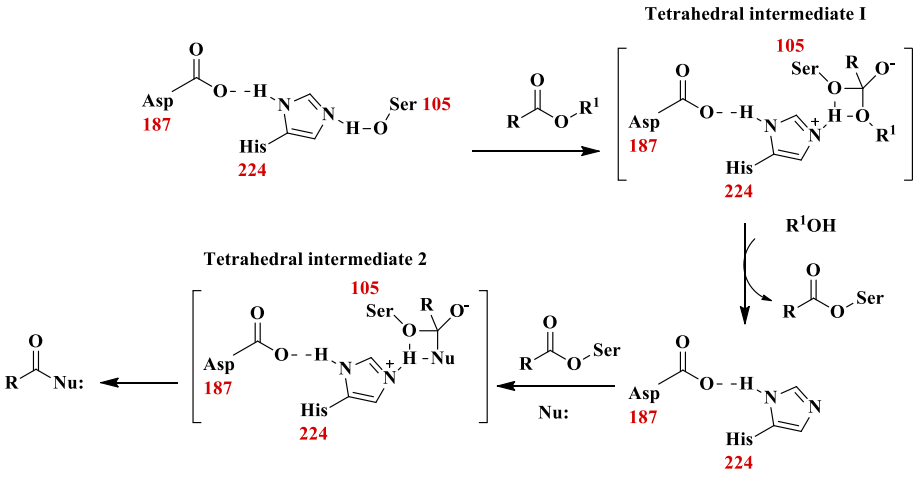

Scheme 1. The mechanism for the acylation/deacylation reaction catalyzed by CALB.

His224 and Asp187, and a resolved structure by X-ray diffraction (Uppenberg et al., 1994, 1995). Commercially available CALB immobilized on polyacrylic resin defined as Novozyme 435 is particularly useful enzyme, as it demonstrates exceptionally high stability and sound activity in organic solvents at high temperatures. Several reactions have been reported to use CALB, including the Michael addition (Souza et al., 2009; Yuan et al., 2017) which is an unexpected reaction for hydrolytic enzymes. The Michael addition reaction (or 1, 4- addition) plays an important role in organic synthesis, as one of the most crucial methods to form C–C and C–X (X = heteroatom) bonds, owing to its atom-economy and efficiency (Michael, 1887). From the mechanism point of view Michael addition is a nucleophilic addition of a nucleophile to α, β-unsaturated carbonyl compound. When the nucleophile is nitrogen the reaction is called an aza-Michael addition. The aza-Michael additions products are β-amino carbonyl compounds, which are of significance both biologically and synthetically (Magriotis, 2001). So far, most related research within this area have focused on aza-Michael addition incorporating amines as the Michael donor (Dhake et al., 2010; Dutt et al., 2020; Steunenberg et al., 2013). However no research has been devoted to chemo-enzymatic aza--Michael addition involving amide as the Michael donor. Hydrazides are important amide intermediates (Majumdar et al., 2014) specifically due to their contribution to the synthesis of compounds showing biological properties, including antituberculous agent (Isoniazid), HIV inhibitors, inhibitors of myeloperoxidase, glycogen phosphorylase, and pesticides (Kettle et al., 1995). Acyl hydrazides have been known as novel inhibitors of mammalian cathepsin B and cathepsin H (Raghav and Singh, 2014). Up until now, literatures provide mechanistic explanations of lipase catalyzed transesterification or amidation that proceeds through acylation of Ser105 (within the active site of CALB) by appropriate carbonyl compound, giving the acylated intermediate, followed by a nucleophilic attack (an alcohol, amine or water) at the Serine bound carbonyl group, and consequent liberation of the acyl group, giving the desired product (Scheme 1). Both steps proceed via an intermediate structure that has a Serine bound carbon, having a tetrahedral geometry. In seminal papers by Warshel (Schopf and Warshel, 2014; Warshel et al., 1989) and co-workers on the mechanism of protease and lipase, it was proposed enzyme catalyzed the reaction through stabilizing the negative charge of oxyanion hole (consists of Thr40 and Gln 106) and by the electrostatic interaction between Asp187 and the ionized His224 (Warshel et al., 1989). In this research, chemo-enzymatic synthesis of diethyl 2-(2-benzoylhydrazinyl)succinate promoted us to undertake further studies, including computational simulation studies to gain insight into the solvent effect.

2. Results and discussion

To investigate role of CALB as a biocatalyst in the reaction, initially noncommercial Benzhydrazide was treated with an excess amount of *Cis*-diethyl maleate (DEM) in a suspension of commercially available immobilized CALB (Novozyme 435) in hexanes (HEX), under argon at 65–68 °C. The reaction was allowed to stir sluggishly for 48 h, during which the reaction progress was monitored by TLC (Scheme 2). Since a portion of starting substrates remained after 24 h, therefore, the reaction time was extended to 48 h. After 48 h reaction showed a trivial progress, but starting substrates still were not consumed entirely. Once the reaction was deemed complete, the ^{1}H NMR spectrum (Figure 1 & Figure S2) of the purified compound displayed a diagnostic peak at 5.70 ppm, attributing to C*H* in vicinity of NH, which was a hint for structure elucidation of the product. Compound **4** (Scheme 2) was further confirmed by ^{13}C NMR (Figure S3) spectrum and it turned out to be

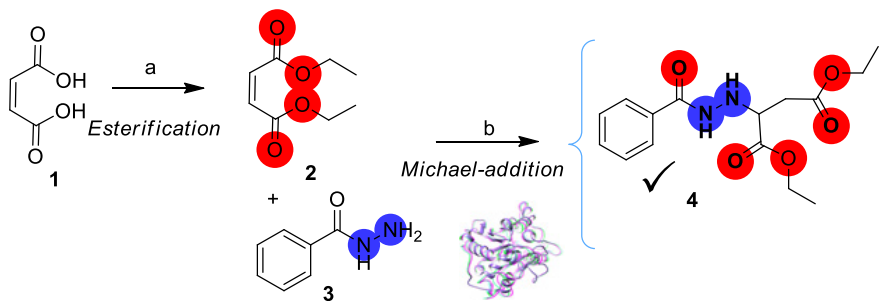

Scheme 2. *Reagents and conditions*: a) EtOH (10.0 equiv, reflux, O/N), b) Novozyme 435 (60 mg), Hexanes (dry), rpm 170, 65–68 °C, Argon atm, 2 days.

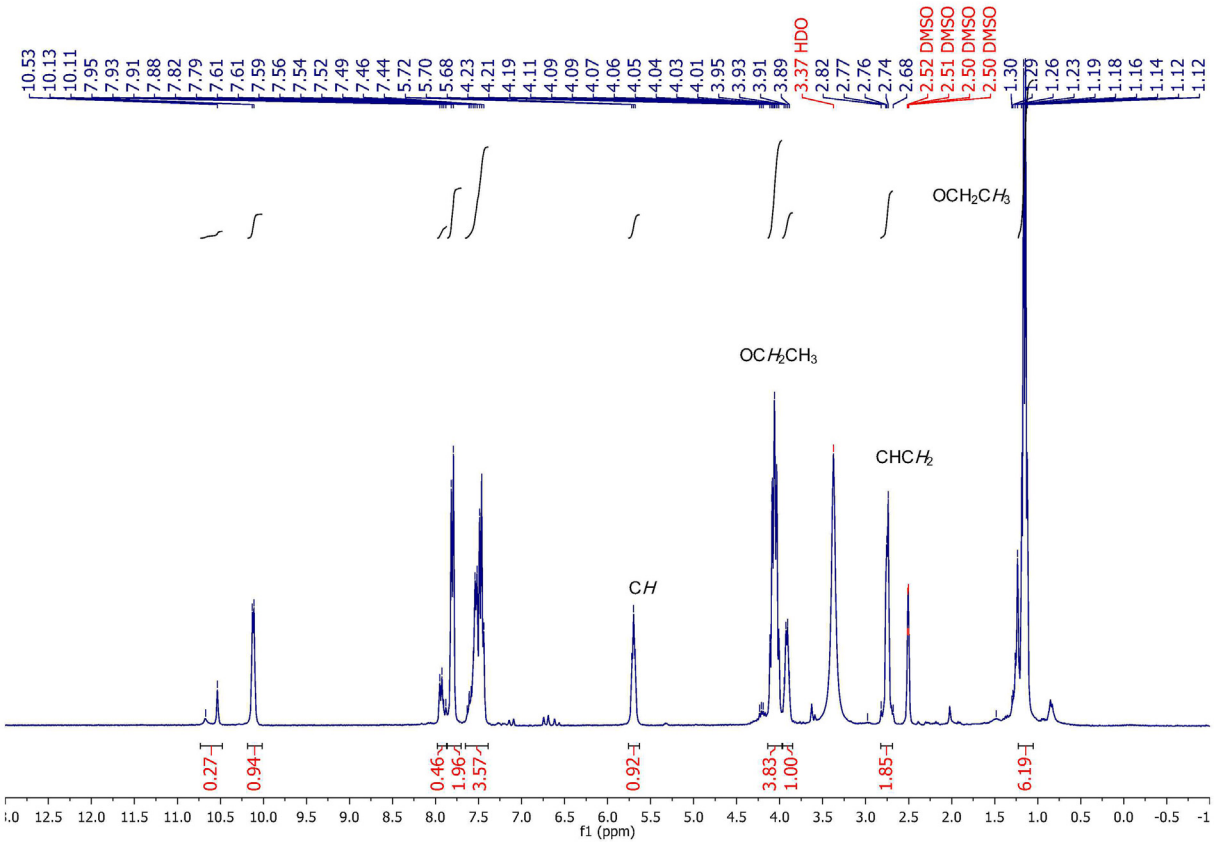

Figure 1. The ^{1}H NMR (mixture of two rotamers) spectrum showing diagnostic peak C*H*NH at 5.70 ppm.

unknown, which was not reported previously. The compound was initially isolated as a transparent glassy solid, which under argon turned into an insoluble solid crystal.

The isolated compound was unstable, and it was decomposed to the corresponding Benzhydrazide a few hours after isolation. According to this results reaction proceeded via regioselective mono adduct of Benzhydrazide and DEM, giving diethyl 2-(2-benzoylhydrazinyl) succinate as a major product. Considering the stereogenic center forged during the reaction optical rotation of the product was measured, which showed a racemic compound with no optical activity. The reaction condition is comparable to the research by Quirós et al. (1995) who treated DEM and/or fumarate with amine in a suspension of CALB in Dioxane. However, under reported conditions no mono adduct product was isolated in either case. To further probe role of enzyme in the reaction, a control experiment was set up, which did not form the compound produced in the presence of enzyme. Additionally, reaction did not proceed when free enzyme was utilized, which can be attributed to the lack of long-term stability. However, immobilized enzyme does not have drawbacks associated with using free enzyme (Hanefeld et al., 2009; Sheldon, 2007; Tran and Balkus, 2011). Ease of handling of the enzyme, as a solid rather than a liquid, facilitates separation from the product, plus enhanced stability towards denaturation by heat or organic solvents. Novozym 435 exhibits optimal activity at 50 °C and functions in the temperature ranging from 10 to 70 °C and at pH values between 7.0 and 9.0. Given enzyme activity within the cited temperature the optimum temperature 65–68 °C was set due to the failure of the reaction at temperatures ranging from 35 °C to 65 °C.

The possibility of undergoing an aza-Michael addition without using any catalyst or solvent was reported for amines previously (Kodolitsch et al., 2020; Ranu et al., 2002). Noteworthy is failure of the reaction to generate the desired product with other solvents, including DCM and THF, which was in line with efficiency and activity of CALB in HEX as the nonpolar solvent compared with polar-solvents reported in literature (Dutta Banik et al., 2016). The choice of organic solvent is often crucial in the reaction outcome (Russell and Klibanov, 1989). Several factors have been proposed to affect enzyme activity in organic solvents, including enzyme pliability, competitive inhibitory by solvent molecules, stability of the transition state, substrate solubility and hydration level (Dutta Banik et al., 2016). Although these factors and parameters have provided some insight, still the complexity of the impact of organic solvent on the enzymatic reaction remains ambiguous. One reason is that only limited number of research attempted to conduct experiments and simulations in parallel to ensure that the reaction conditions are virtually comparable. To this end, we decided to combine experimental results with MD simulations to gain a molecular insight into organic solvent molecules effect on the catalytic activity of CALB at high temperature in a Michael addition reaction.

3. Materials and methods

The ^{1}H NMR spectra were recorded at 300 MHz, or at 500 MHz spectrometer and were reported in ppm relative to the solvent reference ($CDCl_3$, δ 7.26 ppm; DMSO, δ 2.54 ppm). ^{13}C NMR spectrum was recorded at 75 MHz. Chemical shifts for ^{13}C NMR spectrum were reported in parts per million (ppm) downfield relative to the center line of the triplet of DMSO at 39.5 ppm. Coupling constants (*J*) were quoted in Hertz (Hz). Unless otherwise noted, commercially available chemicals were used as received. Novozyme 435 was a generous gift from Novozymes (Denmark).

3.1. Experimental results

Synthesis of *Cis*-diethyl maleate (DEM) (**2**): To a flask containing EtOH (10 equiv, 86 mmol, 4.0 mL) maleic acid (1.0 equiv, 8.6 mmol, 1.0

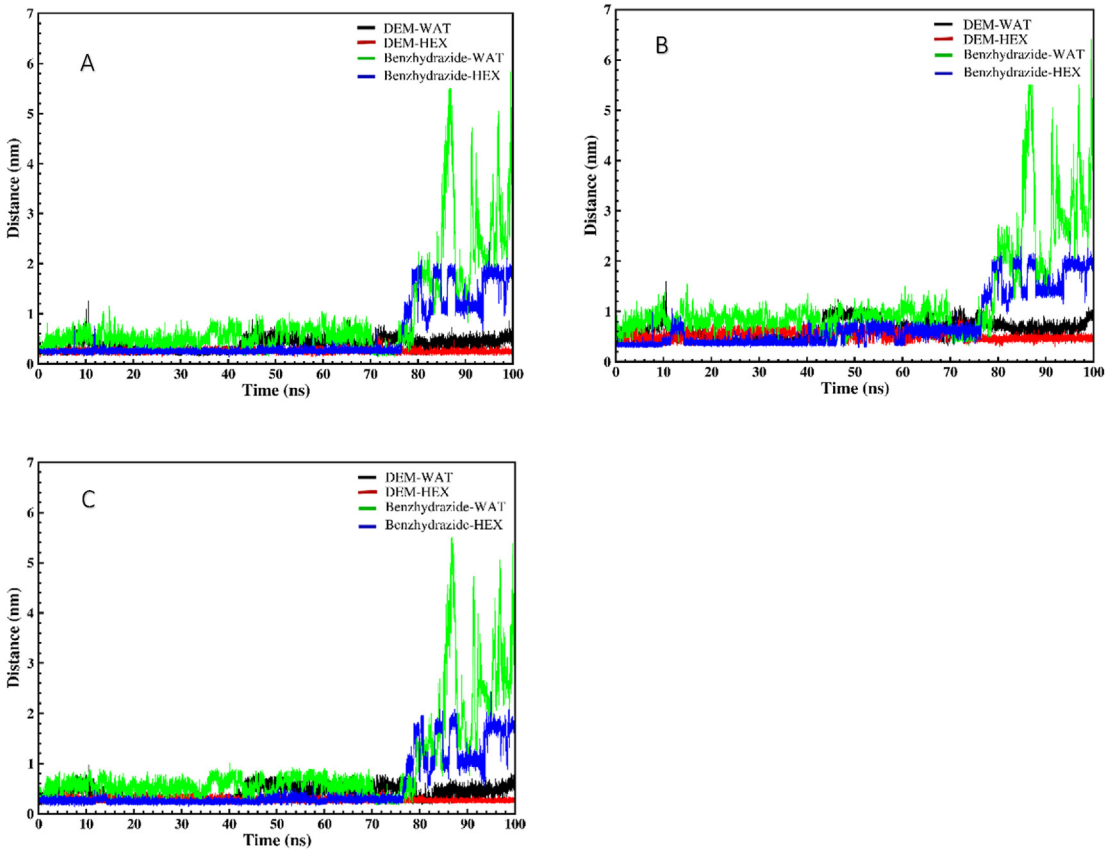

Figure 2. (**A**) The minimum distance changes between the ligands and Ser105; (**B**) The minimum distance changes between the carbonyl group (C=O) of both ligands with respect to hydroxyl group (OH) of Ser105; (**C**) The minimum distance changes between the ligands and His224.

g) was added, followed by catalytic amount of H_2SO_4. Reaction was allowed to reflux for 13–15 h. After reaction was deemed complete via TLC, reaction mixture was concentrated under reduced pressure, diluted with EtOAc, and dried over Na_2SO_4. Concentration of the solvent in *vaccue* yielded a crude which was purified via flash chromatography (25% EtOAc: Hexanes) to produce the *title* compound as a colorless oil in 80% (1.1 g) yield. The data were in agreement with literature values (Kaplaneris et al., 2017). **^{1}H NMR** (500 MHz, $CDCl_3$, δ ppm) 6.25 (s, 2 H), 4.24 (q, J_{Cis} = 7.1 Hz, 4 H), 1.3 (t, J_{Cis} = 7.1 Hz, 6 H).

Synthesis of Diethyl 2-(2-benzoylhydrazinyl) succinate (**4**): To a vessel pre-charged with Argon Benzhydrazide (0.5 mmol, 0.68 g), DEM (0.75 mmol, 0.13 g), and Novozyme 435 (60 mg) were added. To this, dry hexane was added, and the reaction was allowed to stir at 65–68 °C for two days. Upon completion of the reaction, the enzyme was filtered through a short plug of Celite, washed with EtOAc and the solvent was evaporated under reduced pressure. Then, crude was purified using neutralized column chromatography eluting with a solvent gradient of 20 % EtOAc/Hexanes to 40 % EtOAc/Hexanes. The *title* compound was obtained as a white glassy solid in 60 % (92 mg) yield. **^{1}H NMR** (300 MHz, DMSO, δ ppm) (br d, 10.12, 1 H), (2 br d, 7.94 & 7.80, 5 H), 5.69 (t, 1 H), 4.06 (m, 4 H), 3.91 (m, 1 H), 2.5 (br s, 1 H), 1.24 (br d, 1 H), 1.15 (m, 6 H), **^{13}C NMR** (75 MHz, DMSO, δ ppm) 171.4, 170.8, 166.3, 133.2, 132.0, 128.8, 127.9, 127.6, 61.1, 60.6, 59.2, 14.4, 14.3. **ESI-MS** Calcd. for $[C_{15}H_{20}N_2O_5]$ m/z = 308.14 found 308.3.

3.2. Computational method

The computational part of this study involves following sections: a) optimization and structural analyses of the docked poses via molecular docking, and b) MD simulation studies to verify the reliability of the results. The AutoDock 4.2 (Morris et al., 2009) software was used for molecular docking studies and MGLTOOLS (Forli et al., 2016) software for visualization and preparation of input files and output files analysis (Figures S4 & S6, Tables S1, S2 & S3). The Chimerax (Goddard et al., 2018) and LigPlus (Laskowski and Swindells, 2011) were used for 3D and 2D structure visualization (Figures S5 & S7), respectively. Details of system set up for the docking studies are explained in Supplementary Information associated with this manuscript.

3.3. Molecular dynamics simulation studies

In order to understand the effect of HEX on the CALB activity in mediating the reaction, we performed a series of molecular dynamics simulations of CALB in HEX and WAT. The latter simulation was used as a reference to highlight structural changes in CALB when is exposed to organic medium. In the current study, classical MD simulations were employed, without considering the transition state, as this would require quantum mechanical calculations. Our analyses were directed towards the geometrical properties of CALB, and interactions of substrate/solvent/water molecules within the CALB active site region. In the following sections, we initially analyze the position of each ligand within the active site over the course of simulations, and overall structure and flexibility of CALB in HEX and WAT. Then, interaction between CALB and solvent molecules, and interaction between substrate and solvent molecules are investigated. Lastly, based on distance analyses data together with level of stability of each ligand throughout simulation we study of whether it makes a difference if ligand binding order to the active site is swapped?

3.4. System setup and MD simulations

The CALB crystal structure was taken from the Protein Data Bank (PDB ID: 1TCA; resolution 1.55 Å). The enzyme is a monomer and

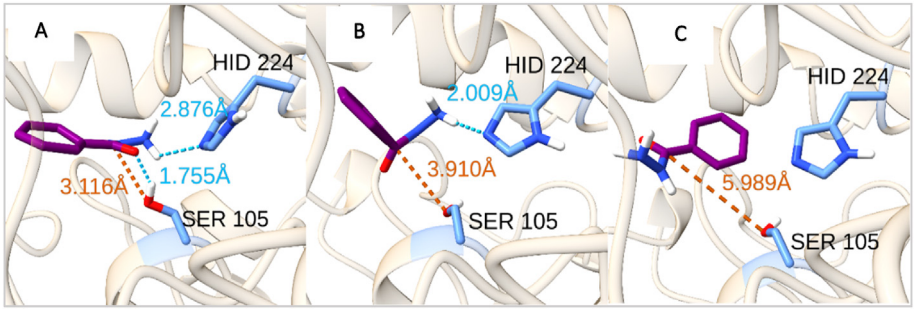

Figure 3. The status of Benzhydrazide in the active site pocket in HEX at (**A**) 0 ns (**B**) 40 and (**C**) 75 ns.

consists of 317 amino acids. The active site consists of a catalytic triad formed by Ser105, His224, and Asp187. The protonation state of the ionizable residues was defined at pH 7. The protonation states of the titratable residues were checked using the propKa module of the PDB2PQR (Rostkowski et al., 2011). The Asp134 along with His224 in the catalytic triad were protonated. The Lys and Arg residues were positively charged whereas Asp (except Asp134) and Glu residues were negatively charged. The histidine (His 224) that is a part of the catalytic triad was treated neutral with the proton on N_δ and was labeled as HID in all four simulations. Additionally, the disulfide bonds in CALB were defined. The MD simulations were performed by GROMACS 2021.2 software (Van Der Spoel et al., 2005) using ff99SB + ILDN force field (Lindorff-Larsen et al., 2010). The protein was solvated using gmx solvate software in a cubic box of TIP3P (Mark and Nilsson, 2001) water molecules and Hexanes with 10 Å radius. Then the systems were energy minimized for 5000 cycles, using the steepest descent (Fliege and Svaiter, 2000) algorithm together with the conjugate gradient method to remove any bad interaction between atoms. The minimized systems were first gradually heated from 0 to 338 K over 200 ps using a Langevin thermostat at constant condition (NVT) and equilibrated with a time step of 2 fs, and then systems were equilibrated for 400 ps at constant pressure (1.0 atm) (NPT) with a time step of 2 fs. The MD simulations were done employing periodic boundary conditions adopting a 10 Å cut-off for non-bonded interactions, while non-bonded electrostatic interactions were carried out at a distance of 10 Å, adhering to the Particle Mesh Ewald (PME) method (Gilson et al., 1988). The SHAKE algorithm (Ryckaert et al., 1977) was used to fix all covalent bonds involving hydrogen atoms. Finally, simulations were conducted at 338 k over 100 ns, during which data were saved after every 8.0 ps. The *Antechamber* (Wang et al., 2001) software available in *AmberTools* (Macke et al., 2010) package was utilized for parametrization of ligands, including DEM, Benzhydrazide and SEH. Generated parameters were then converted to GROMACS format via ACPYPE (Sousa da Silva and Vranken, 2012) script. The calculated density for optimized HEX solvent was 0.64 ± 0.32 g/cm^{-3}. The number of HEX molecules in interaction with DEM, Benzhydrazide, and SEH was 1598, 1499 and 1495 respectively. When simulation was performed in aqueous medium the simulation box included 14,844 WAT molecules for simulation involving DEM and 14848 WAT molecules for simulations involving Benzhydrazide respectively.

3.5. Distance analyses of ligands with respect to active site residues (Ser105 & His224)

The minimum distance changes and/or variation between center of mass of ligands (*i.e.* DEM and Benzhydrazide) and center of mass Ser105 and His224 over the course of simulations (*i.e.* 100 ns) were investigated. As can be seen in Figure 2A, DEM in HEX (red) demonstrated stability within the active site pock, maintaining a 0.2 nm distance to Ser105 throughout simulation. While DEM minimum distance to Ser105 in WAT (black) showed a distance around 0.2 nm within the first 42 ns, it distanced further afterwards showing 0.5 nm distance. The distance remained unchanged until the end of simulation, which indicated ligand has detached from the cavity. Probing Benzhydrazide status when simulation was conducted in HEX (blue) showed ligand stability until 76 ns, staying at 0.2 nm distance with respect to Ser105. Afterwards, the distance between the ligand and Ser105 rose significantly, reaching 1.6 nm after 80 ns. Likewise, minimum distance changes of Benzhydrazide with respect to Ser105 in aqueous medium, *i.e.* WAT (green), displayed a distance at around 0.6 nm within the first 78 ns, but it dramatically increased its distance from Ser105 afterwards, showing 5.8 nm distance at the end of simulation, which suggested that ligand was pushed out of the cavity.

Based on the discussed mechanism in Scheme 1 the carbonyl groups (C=O) of DEM and Benzhydrazide should be close to Ser105 for an ester bond formation. Due to this, the distance changes for the carbonyl group of both ligands with respect to hydroxyl group of Ser105 were investigated (Figure 2B). As can be seen in Figure 2B hydroxyl group of Ser105 has a closer distance to C=O of DEM in HEX compared with C=O of Benzhydrazide carbonyl group in HEX. Based on distance analysis we can deduce that DEM is more willing for covalent bonding formation with Ser105 compared to Benzhydrazide. In an analogous fashion the minimum distance changes and/or variation between center of mass of ligands and His224 was investigated, which showed similar behavior to

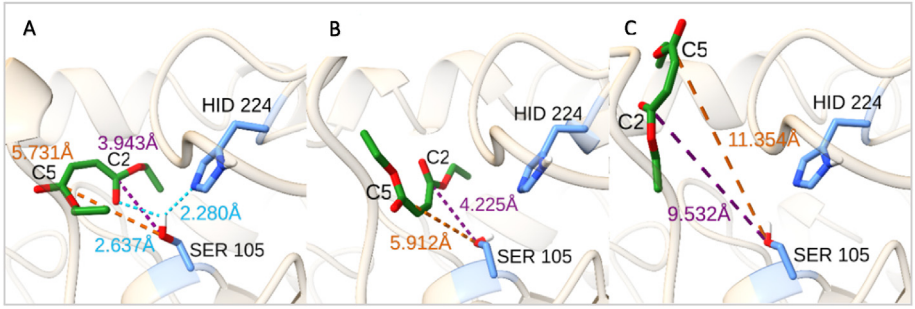

Figure 4. DEM status in the active site pocket in WAT (**A**) 0 ns (**B**) 40 ns (**C**) 100 ns.

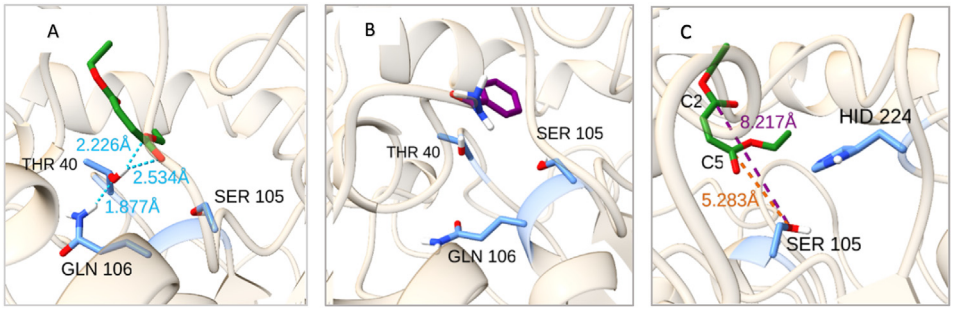

Figure 5. (**A**) DEM hydrogen bonding with Thr40, and its position with regard to Gln106 and Ser105 in HEX at the end of simulation (100 ns); (**B**) Benzhydrazide status with regard to residues forming oxyanion holes (Thr40, Gln106); (**C**) The bond length between C2 and C5 of DEM and oxygen atom of hydroxyl group of Ser105.

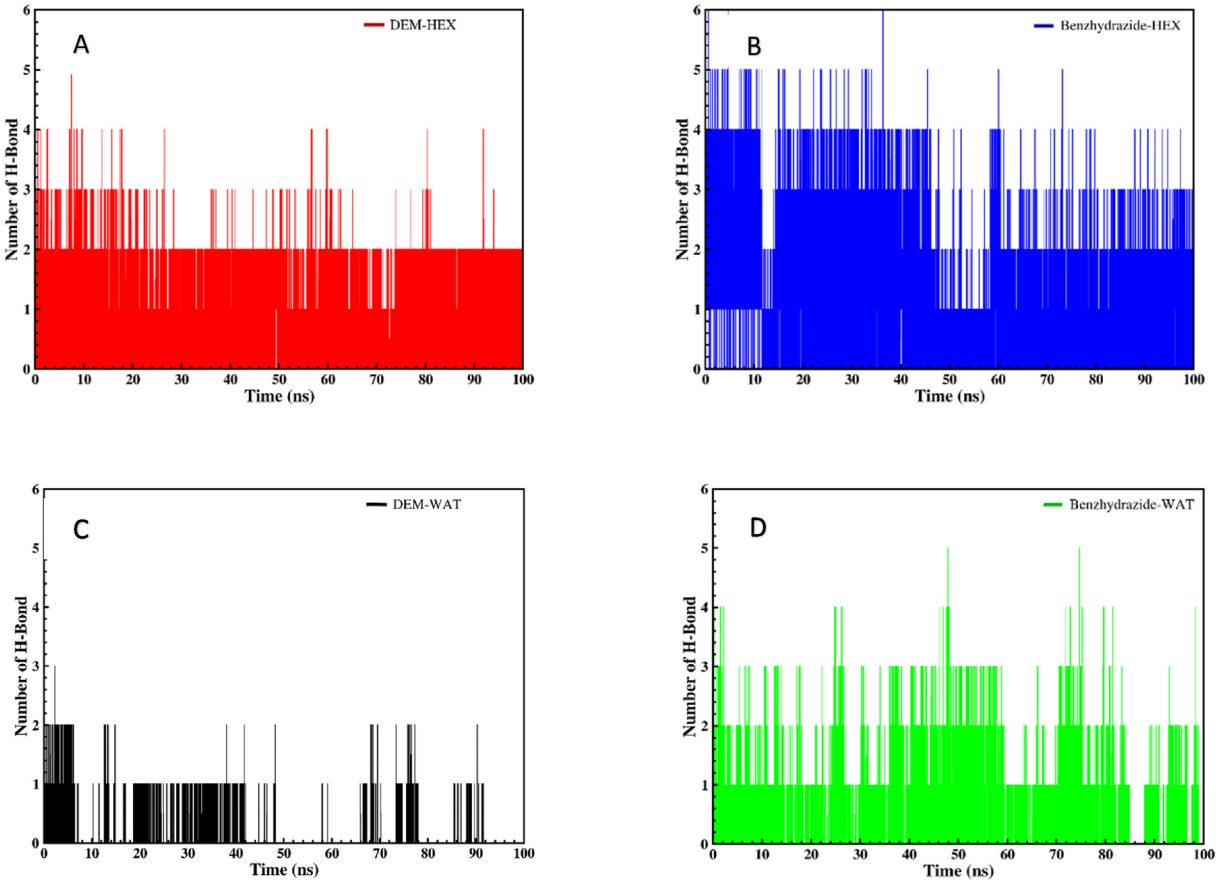

Figure 6. Overall hydrogen bonding interactions between (**A**) DEM and CALB in HEX (**B**) Benzhydrazide and CALB in HEX (**C**) DEM and CALB in WAT and (**D**) Benzhydrazide and CALB in WAT throughout simulation.

those of observed for the minimum distance changes between ligands and Ser105 (Figure 2C).

The Benzhydrazide orientation and distance with respect to active site residues at 0, 40, 75 ns in HEX are shown in Figure 3. While at 0 ns the ligand forms hydrogen bonding with Ser105 and His224 with the hydrogen bonds length 1.755 Å and 2.876 Å respectively, these bonds were dissociated at 40 ns and 75 ns indicating ligand detachment from the active site.

Likewise, DEM orientation and distance with respect to active site residues in WAT is shown in Figure 4. As can be seen DEM was stable within the active site pocket and was engaged with Ser105 through hydrogen bonding with the hydrogen bond length 2.637 Å at 0 ns. Additionally, one hydrogen bonding was formed between Ser105 and His224 with 2.280 Å length. Nevertheless, the hydrogen bonds were dissociated at 40 ns and the distance between carbonyl groups of DEM (*i.e.* C2 and C5) and oxygen atom of hydroxyl group of Ser105 (*i.e.* C2–O and C5–O) increased to 9.532 Å and 11.354 Å respectively.

As for DEM status in HEX it can be seen (Figure 5, **A**) the ligand forms two hydrogen bonding with Thr40 at the end of simulation (100 ns) with hydrogen bond length 2.534 Å and 2.226 Å. Thr40 and Gln106 form the so-called oxyanion hole which is a pocket in the active site stabilizing the transition state negative charge. It has been proposed that catalysis proceeds via activation of the carbonyl substrate through the oxyanion hole. In contrast Benzhydrazide shows no hydrogen bonding with these residues from 75 ns onwards (Figure 5, **B**). The bond length between C2 and C5 of DEM and oxygen atom of hydroxyl group of Ser105 namely C2–O and C5–O (Figure 5, **C**) was 5.283 Å and 8.217 Å respectively, at the end of simulation (100 ns).

Hydrogen bonding plays an important role in ligand stabilization within the active site pocket; the more hydrogen bonding interactions the

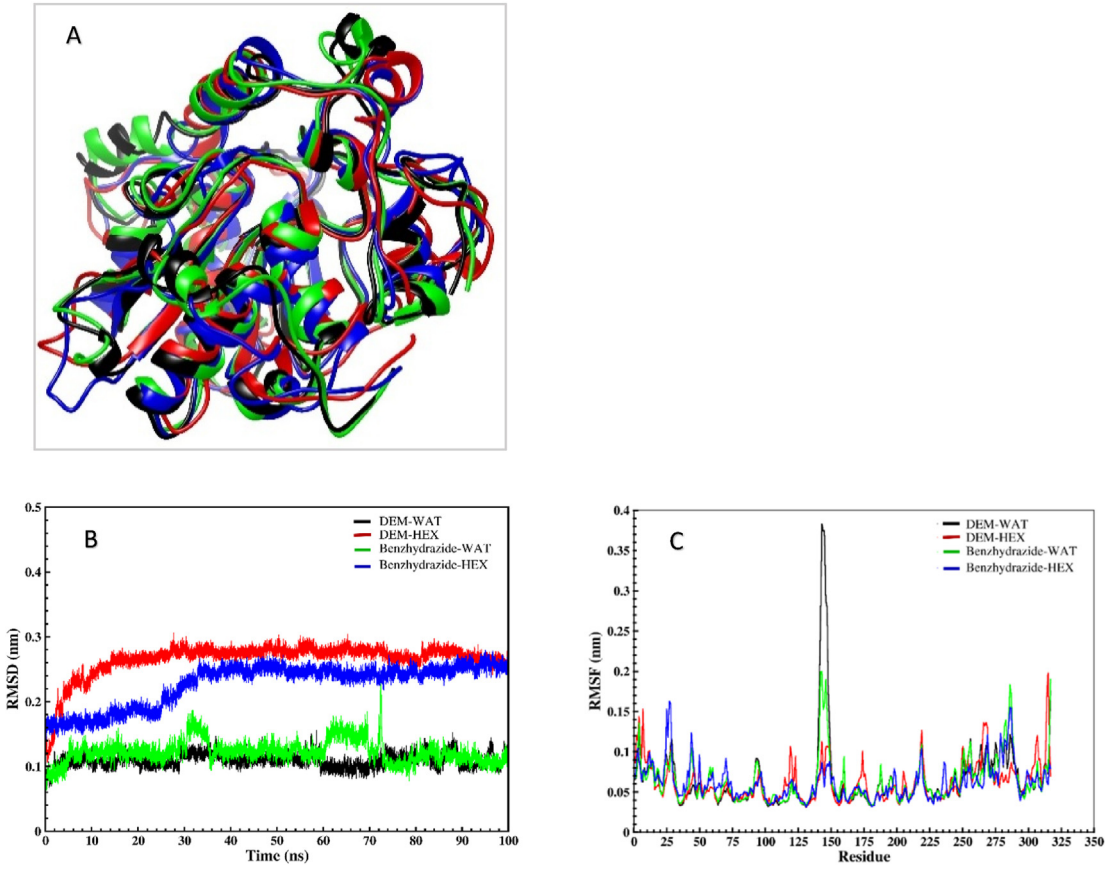

Figure 7. (**A**) Superimposition of the last frame of CALB in HEX (red & blue) with the last frame of CALB in WAT (black & green); (**B**) The RMSD changes throughout simulation for all four systems; (**C**) The RMSF of all amino acid residues of CALB in interaction with DEM and Benzohydrazide both in HEX and WAT.

more stable is the ligand in the active site. The hydrogen bonding interactions between ligands and residues of active site in HEX and WAT are shown in Figure 6. As can be seen both ligands formed more hydrogen bonding in HEX (Figure 6A and B) while in comparison the number of hydrogen bonding decreased in WAT for both ligands (Figure 6C and D). Nevertheless, number of hydrogen bonding does not necessarily indicate that the ligand is in the active site and vice versa.

3.6. Structure and flexibility of CALB in aqueous and nonaqueous solvent

The superimposed backbone structures of CALB from the last frame of each simulation (*i.e.* 100 ns) in interaction with DEM and Benzhydrazide both in HEX and WAT is shown in Figure 7A. Altogether, it appears the backbone structure was maintained in the HEX and WAT throughout simulations and it only showed minor differences, which can be distinctively observed at regions from 13-18, 19–22, 268–276 amino acid residues in WAT. To assess stability and geometrical features of CALB in HEX and WAT several factors including root-mean-square deviation (RMSD), radius of gyration (Rg), and solvent accessible surface area (SASA) were calculated. The RMSD of the C^{α} on the protein backbone with respect to the initial structure has been shown in Figure 7B. The higher RMSD value the more structural changes (*i.e.* the overall topology of the protein) with respect to the initial structure. Thus, CALB underwent more structural changes relative to its initial structure in HEX (red and blue) compared to WAT (black and green) Figure 7B, indicating its higher RMSD value in HEX. To investigate the flexibility of CALB in HEX and WAT one of the appropriate parameters to calculate is the root mean square fluctuation (RMSF). The RMSF of all amino acid residues of CALB in HEX and WAT in interaction with DEM and Benzhydrazide throughout simulation is shown in Figure 7C. According to Figure 7C CALB shows

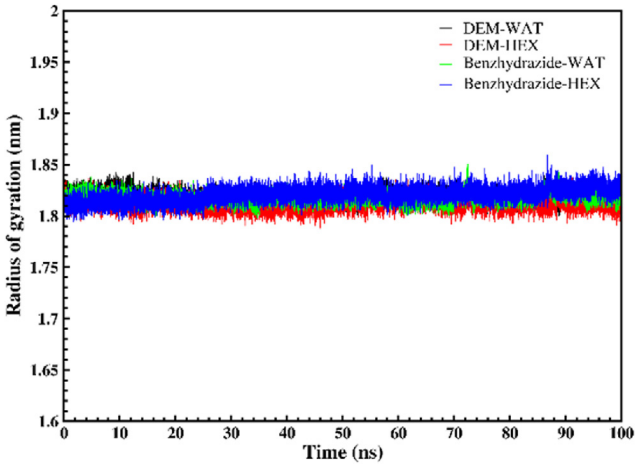

Figure 8. Radius of gyration (Rg) in WAT and HEX.

lesser flexibility when ligands were in HEX compared to when they are in WAT. One of the main differences of RMSF in HEX and WAT was high fluctuation of the residues 138–150 in WAT. The cited region (138–150) is indeed α5 region located at the entrance of the pocket in CALB. The high flexibility of α5 helix at region 138–152 is of importance for CALB function as reported before (Skjøt et al., 2009). Additionally, amino acid residues from 168-187 and 184–207 corresponding to α10 helix and loop L11 respectively, located in vicinity of α5 region, did not show tangible fluctuation. Overall, it can be deduced that decrease in fluctuation of the α5 region gave rise to stability of DEM in active site pocket.

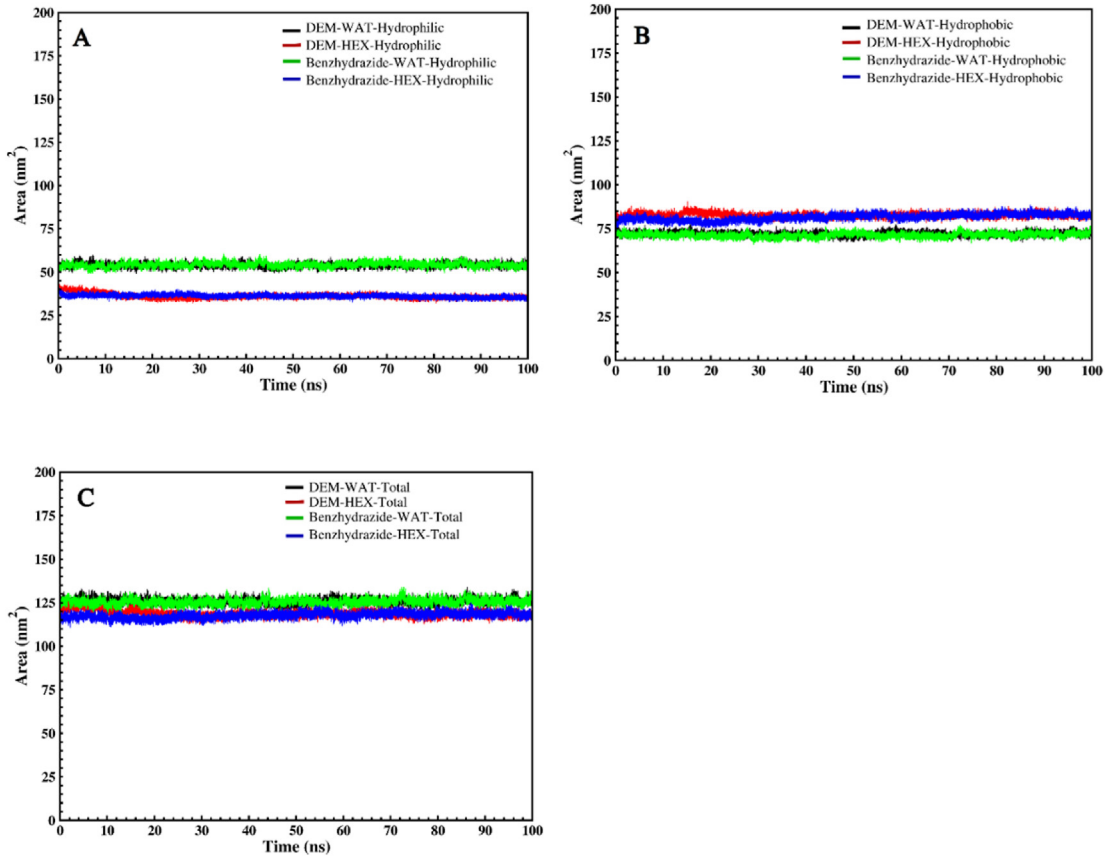

Figure 9. (**A**) Hydrophilic solvent accessible surface area (SASA) of CALB in WAT and HEX; (**B**) Hydrophobic solvent accessible surface area (SASA) in HEX and WAT; (**C**) The total (Hydrophobic and Hydrophilic) solvent accessible surface area of CALB in WAT and HEX.

Table 1. Binding free energies calculated for DEM and Benzhydrazide.

Unit: kJ/mol	ΔG_{Elec}	ΔG_{vdw}	ΔG_{polar} (WAT)	ΔG_{apolar} (HEX)	ΔG_{MMPBSA}
CALB-DEM	−15.679	−120.891	44.800	−12.176	−103.946
CALB-Benzhydrazide	−16.921	−104.199	41.584	−9.325	−88.861

One of the indicators of protein structure compactness is the radius of gyration (Lobanov et al., 2008) (Rg) which is affected by the medium in which the protein is placed. It represents the accessible surface of the protein as a result of interaction with solvent. On the basis of this definition, it appears that the Rg value for CALB in interaction with Benzhydrazide in HEX (blue) has increased from 1.81 nm at the beginning of simulation with a slight increase to 1.82 nm at the end of simulation (Figure 8). Overall the figure showed a relatively constant Rg value for all four systems throughout simulation. In continuation solvent accessible surface area (SASA) of CALB both in HEX and WAT was explored. The SASA slowly climbed by increasing polarity from HEX to WAT (Figure 9A). Polar solvents such as water molecules interact with polar and charged residues of CALB, exposing them to the solvent. In comparison, in nonpolar solvents like Hexane, exposed polar/charged residues are hidden inside the enzyme to reduce the energy required for exposing polar/charged residues to the hydrophobic solvent. As a result, the hydrophilic surface area declines by increasing hydrophobicity of the

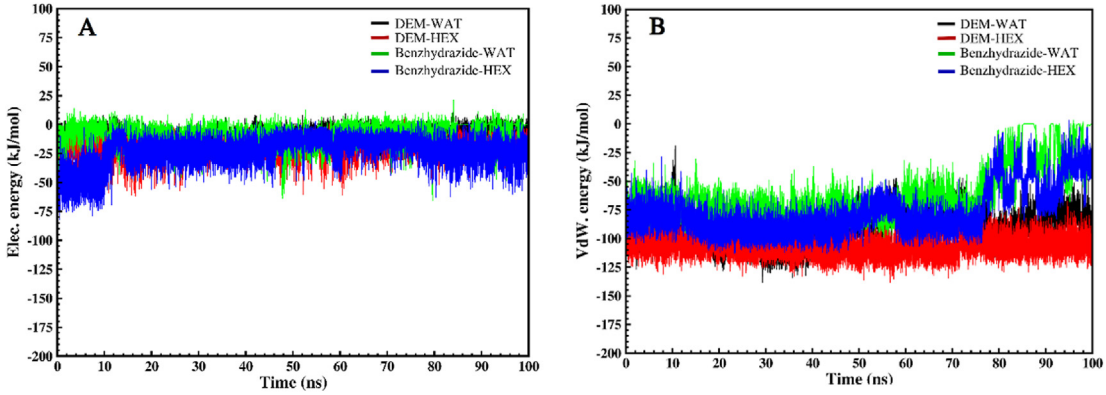

Figure 10. (**A**) Electrostatic and energy changes for CALB-DEM and CALB-Benzhydrazide and (**B**) van Der Waals energy changes for CALB-DEM and CALB-Benzhydrazide

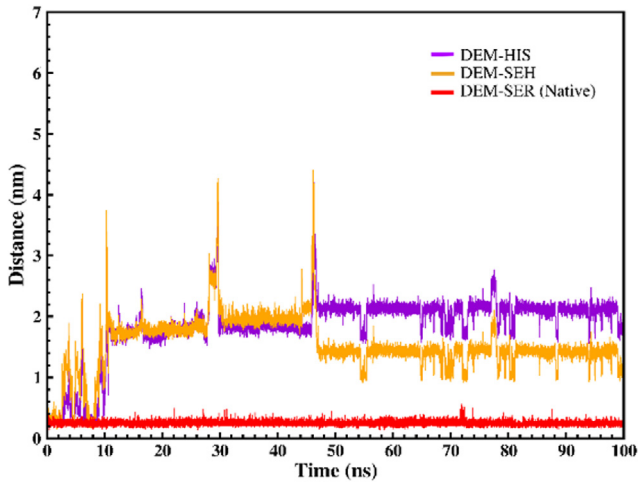

Figure 11. The minimum distance changes between center of mass DEM and His224, as well as DEM and SEH in HEX.

solvent (Figure 9B), which is also in line with reports by others (Li et al., 2010; Peters et al., 1996). According to Figure 9C the total accessible surface (*i.e.* hydrophobic and hydrophilic areas) was slightly more in aqueous medium compared to HEX regardless of the ligand.

3.7. Solvents effect on the CALB surface

The inhibitory effect of solvent molecules on reaction is obtained by the calculation of the binding free energy of substrate and solvent molecules to the active site pocket. Thus, ligand affinity to the protein was estimated by its binding free energy. We utilized *MMPBSA* (Homeyer and Gohlke, 2012) (g_mmpbsa script for GROMACS (Kumari et al., 2014)) to estimate binding free energy of DEM to the active site pocket. To calculate free energy we opted for 400 frames from the stable regions of the simulation (*i.e.* 60-100 ns) for DEM and 300 frames (*i.e.* 20-50 ns) for Benzhydrazide. As can be seen in Table 1. The van der Waals energy (ΔG_{vdw}) was the main source for ligand binding to the active site pocket showing −120.891 and −104.199 kJ/mol values compared with electrostatic energies with −15.679 and −16.921 kJ/mol values for DEM and Benzhydrazide respectively.

Also polar solvation energy (ΔG_{polar}) and non-polar solvation energy (ΔG_{apolar}) were calculated for both ligands, and the results are collected in Table 1. Accordingly, required energy for ligand (both ligands) solvation in HEX was significantly lower than it was required in WAT (positive ΔG indicates unfavorable binding). Binding free energy values for DEM (−103.946) and Benzhydrazide (−88.861) obtained via *MMPBSA* (Homeyer and Gohlke, 2012) method indicate the relative free energy without considering entropy. Because van Der Waals energy plays a crucial role in binding the ligand to the protein, we therefore investigated the van Der Waals energy changes throughout simulation for CALB-DEM and CALB-Benzhydrazide both in WAT and HEX. As Figure 10A demonstrates the electrostatic energy for CALB-DEM in WAT (black) and CALB-Benzhydrazide in WAT (green) was close to zero while it was around −50 kJ/mol in HEX for both ligands. In comparison van Der Waals energy for CALB-DEM in both WAT and HEX was around −100 kJ/mol (Figure 10B) with fluctuation in WAT (black), indicating that DEM dissociated from the CALB, but it became stable in HEX (red) after 15 ns. The van Der Waals energies for Benzhydrazide-CALB in WAT (green) and Benzhydrazide-CALB in HEX (blue) fluctuated between −50 to −75 kJ/mol, again indicating ligand dissociation from the enzyme.

3.8. Does it make a difference if "ligand binding order" to the active site is swapped?

To probe whether DEM could be still stable if it enters and binds to the active site pocket as the second substrate (rather than the first substrate), Benzhydrazide was covalently bound to the Ser105, and the built complex (*i.e.* Ser105-Benzhydrazide) was labeled as SEH. The reason is that Benzhydrazide was not stable within the active site pocket through non-bonded interactions, and therefore it was pushed out of the active site both in WAT and HEX (after 76 ns) as is shown in Figure 2A and C. However, the made-up covalent bond between Benzhydrazide and CALB hindered Benzhydrazide dissociation from the active site. Then, DEM binding to the Ser105-benzyhdrazide complex was analyzed by docking studies. Afterwards, the complex was used for MD simulation in HEX at 338 k. As for His224, the proton on both ND1 and NE2 were selected in the simulation of tetrahedral Intermediate I following literature (Li et al., 2010). As it was shown previously DEM maintained a fixed distance towards Ser105, when it was bound to the active site as the first substrate (Figure 11, red), however it was not stable in the active site when it was bound as the second substrate (orange), and it detached completely from the enzyme after 10.0 ns.

To prove DEM exit from the active site we probed the distance between DEM and His224, since His224 is located at the surface of the active site compared to Ser105, which is located inside the active site pocket. Thus, according to the DEM-His distance analysis (purple) the ligand was pushed out of the active site, showing 3.6 nm distance from the His224 around 2.0 ns. This observed instability for DEM-SEH rationalizes the priority of DEM binding to the active site over Benzhydrazide binding to the active site.

3.9. Concluding remarks

To evaluate the influence of Hexane as the organic solvent on the activity of CALB at the molecular level we carried out a series of MD simulations of CALB in hexane. We also included a simulation of CALB in water as a reference to be able to compare the structural changes in CALB when is exposed to organic medium. From geometrical analyses we deduced that the overall conformation of CALB was stable, and did not show major difference in water and hexane.

The binding free energy of substrate and solvent molecules to the active site pocket showed that required energy for both ligands solvation in hexane was significantly lower than it was required in water. The ligand binding order also turned out to have crucial role in proceeding of the reaction, as when order of ligands was swapped through built-up covalent bond between the Benzhydrazide and Ser105 (i.e., SEH) DEM was not stable in the active site as the second ligand and was pushed out of the active site. The formation of desired molecule in hexane despite instability of Benzhydrazide from 75 ns onwards could be interpreted by the formation of DEM-CALB complex, as once DEM was engaged with the CALB, therefore the Benzhydrazide could easily interact with DEM-CALB complex to furnish desired target molecule.

Declarations

Author contribution statement

Zohreh Nazarian: Conceived and designed the experiments; Performed the experiments; Analyzed and interpreted the data; Contributed reagents, materials, analysis tools or data; Wrote the paper.

Seyed Shahriar Arab: Analyzed and interpreted the data; Contributed reagents, materials, analysis tools or data.

Funding statement

This work was supported by Iran's National Elites Foundation.

Data availability statement

Data associated with this study has been deposited at ChemRxiv.

Declaration of interests statement

The authors declare no conflict of interest.

Additional information

Supplementary content related to this article has been published online at https://doi.org/10.1016/j.heliyon.2022.e10336.

References

Angajala, G., Pavan, P., Subashini, R., 2016. Lipases: an overview of its current challenges and prospectives in the revolution of biocatalysis. Biocatal. Agric. Biotechnol. 7, 257–270.

Busto, E., Gotor-Fernández, V., Gotor, V., 2010. Hydrolases: catalytically promiscuous enzymes for non-conventional reactions in organic synthesis. Chem. Soc. Rev. 39 (11), 4504–4523.

Dhake, K.P., Tambade, P.J., Singhal, R.S., Bhanage, B.M., 2010. Promiscuous Candida antarctica lipase B-catalyzed synthesis of β-amino esters via aza-Michael addition of amines to acrylates. Tetrahedron Lett. 51 (33), 4455–4458.

Dutt, S., Goel, V., Garg, N., Choudhury, D., Mallick, D., Tyagi, V., 2020. Biocatalytic Aza-Michael addition of aromatic amines to enone using α-amylase in water. Adv. Synth. Catal. 362 (4), 858–866.

Dutta Banik, S., Nordblad, M., Woodley, J.M., Peters, G.H., 2016. A correlation between the activity of Candida antarctica lipase B and differences in binding free energies of organic solvent and substrate. ACS Catal. 6 (10), 6350–6361.

Dwivedee, B.P., Soni, S., Sharma, M., Bhaumik, J., Laha, J.K., Banerjee, U.C., 2018. Promiscuity of lipase-catalyzed reactions for organic synthesis: a recent update. ChemistrySelect 3 (9), 2441–2466.

Fliege, J., Svaiter, B.F., 2000. Steepest descent methods for multicriteria optimization. Math. Methods Oper. Res. 51 (3), 479–494.

Forli, S., Huey, R., Pique, M.E., Sanner, M.F., Goodsell, D.S., Olson, A.J., 2016. Computational protein–ligand docking and virtual drug screening with the AutoDock suite. Nat. Protoc. 11 (5), 905–919.

Gilson, M.K., Sharp, K.A., Honig, B.H., 1988. Calculating the electrostatic potential of molecules in solution: method and error assessment. J. Comput. Chem. 9 (4), 327–335.

Goddard, T.D., Huang, C.C., Meng, E.C., Pettersen, E.F., Couch, G.S., Morris, J.H., Ferrin, T.E., 2018. UCSF ChimeraX: meeting modern challenges in visualization and analysis. Protein Sci. 27 (1), 14–25.

Hanefeld, U., Gardossi, L., Magner, E., 2009. Understanding enzyme immobilisation. Chem. Soc. Rev. 38 (2), 453–468.

Homeyer, N., Gohlke, H., 2012. Free energy calculations by the molecular mechanics Poisson–Boltzmann surface area method. Mol. Inf. 31 (2), 114–122.

Kaplaneris, N., Bisticha, A., Papadopoulos, G.N., Limnios, D., Kokotos, C.G., 2017. Photoorganocatalytic synthesis of lactones via a selective C–H activation–alkylation of alcohols. Green Chem. 19 (18), 4451–4456.

Kettle, A.J., Gedye, C.A., Hampton, M.B., Winterbourn, C.C., 1995. Inhibition of myeloperoxidase by benzoic acid hydrazides. Biochem. J. 308 (2), 559–563.

Kodolitsch, K., Gobec, F., Slugovc, C., 2020. Solvent- and catalyst-free aza-michael addition of imidazoles and related heterocycles. Eur. J. Org Chem. 2020 (19), 2973–2978.

Kumari, R., Kumar, R., Lynn, A., 2014. g_mmpbsa—a GROMACS tool for high-throughput MM-PBSA calculations. J. Chem. Inf. Model. 54 (7), 1951–1962.

Laskowski, R.A., Swindells, M.B., 2011. LigPlot+: multiple ligand–protein interaction diagrams for drug discovery. J. Chem. Inf. Model. 51 (10), 2778–2786.

Li, C., Tan, T., Zhang, H., Feng, W., 2010. Analysis of the conformational stability and activity of Candida antarctica lipase B in organic solvents: insight from molecular dynamics and quantum mechanics/simulations. J. Biol. Chem. 285 (37), 28434–28441.

Lindorff-Larsen, K., Piana, S., Palmo, K., Maragakis, P., Klepeis, J.L., Dror, R.O., Shaw, D.E., 2010. Improved side-chain torsion potentials for the Amber ff99SB protein force field. Proteins: Struct., Funct., Bioinf. 78 (8), 1950–1958.

Lobanov, M.Y., Bogatyreva, N.S., Galzitskaya, O.V., 2008. Radius of gyration as an indicator of protein structure compactness. Mol. Biol. 42 (4), 623–628.

Macke, T.J., Svrcek-Seiler, W.A., Brown, R.A., Kolossváry, I., Bomble, Y.J., Case, D.A., 2010. AmberTools users' manual.

Magriotis, P.A., 2001. Recent progress in the enantioselective synthesis of β-lactams: development of the first catalytic approaches. Angew. Chem. Int. Ed. 40 (23), 4377–4379.

Majumdar, P., Pati, A., Patra, M., Behera, R.K., Behera, A.K., 2014. Acid hydrazides, potent reagents for synthesis of oxygen-, nitrogen-, and/or sulfur-containing heterocyclic rings. Chem. Rev. 114 (5), 2942–2977.

Mark, P., Nilsson, L., 2001. Structure and dynamics of the TIP3P, SPC, and SPC/E water models at 298 K. J. Phys. Chem. 105 (43), 9954–9960.

Michael, A., 1887. Ueber die Addition von Natriumacetessig- und Natriummalonsäureäthern zu den Aethern ungesättigter Säuren. J. Prakt. Chem. 35 (1), 349–356.

Morris, G.M., Huey, R., Lindstrom, W., Sanner, M.F., Belew, R.K., Goodsell, D.S., Olson, A.J., 2009. AutoDock4 and AutoDockTools4: automated docking with selective receptor flexibility. J. Comput. Chem. 30 (16), 2785–2791.

Peters, G.H., van Aalten, D.M., Edholm, O., Toxvaerd, S., Bywater, R., 1996. Dynamics of proteins in different solvent systems: analysis of essential motion in lipases. Biophys. J. 71 (5), 2245–2255.

Quirós, M., Astorga, C., Rebolledo, F., Gotor, V., 1995. Enzymatic selective transformations of diethyl fumarate. Tetrahedron 51 (28), 7715–7720.

Raghav, N., Singh, M., 2014. Acyl hydrazides and triazoles as novel inhibitors of mammalian cathepsin B and cathepsin H. Eur. J. Med. Chem. 77, 231–242.

Ranu, B.C., Dey, S.S., Hajra, A., 2002. Solvent-free, catalyst-free Michael-type addition of amines to electron-deficient alkenes. ARKIVOC Online J. Org. Chem. 76–81.

Rostkowski, M., Olsson, M.H., Søndergaard, C.R., Jensen, J.H., 2011. Graphical analysis of pH-dependent properties of proteins predicted using PROPKA. BMC Struct. Biol. 11 (1), 1–6.

Russell, A.J., Klibanov, A.M., 1989. Enzymes in organic solvents. Biochem. Soc. Trans. 17 (6), 1145.

Ryckaert, J.-P., Ciccotti, G., Berendsen, H.J.C., 1977. Numerical integration of the Cartesian equations of motion of a system with constraints: molecular dynamics of n-alkanes. J. Comput. Phys. 23 (3), 327–341.

Schopf, P., Warshel, A., 2014. Validating computer simulations of enantioselective catalysis; reproducing the large steric and entropic contributions in Candida antarctica lipase B. Proteins: Struct., Funct., Bioinf. 82 (7), 1387–1399.

Sheldon, R.A., 2007. Enzyme immobilization: the quest for optimum performance. Adv. Synth. Catal. 349 (8–9), 1289–1307.

Skjøt, M., De Maria, L., Chatterjee, R., Svendsen, A., Patkar, S.A., Østergaard, P.R., Brask, J., 2009. Understanding the plasticity of the α/β hydrolase fold: lid swapping on the Candida antarctica lipase B results in chimeras with interesting biocatalytic properties. Chembiochem 10 (3), 520–527.

Sousa da Silva, A.W., Vranken, W.F., 2012. ACPYPE - AnteChamber PYthon Parser interfacE. BMC Res. Notes 5 (1), 367.

Souza, R.O.M.A.D., Matos, L.M.C., Gonçalves, K.M., Costa, I.C.R., Babics, I., Leite, S.G.F., Oestreicher, E.G., Antunes, O.A.C., 2009. Michael additions of primary and secondary amines to acrylonitrile catalyzed by lipases. Tetrahedron Lett. 50 (17), 2017–2018.

Steunenberg, P., Sijm, M., Zuilhof, H., Sanders, J.P.M., Scott, E.L., Franssen, M.C.R., 2013. Lipase-catalyzed Aza-Michael reaction on acrylate derivatives. J. Org. Chem. 78 (8), 3802–3813.

Tran, D.N., Balkus, K.J., 2011. Perspective of recent progress in immobilization of enzymes. ACS Catal. 1 (8), 956–968.

Uppenberg, J., Hansen, M.T., Patkar, S., Jones, T.A., 1994. The sequence, crystal structure determination and refinement of two crystal forms of lipase B from Candida antarctica. Structure 2 (4), 293–308.

Uppenberg, J., Oehrner, N., Norin, M., Hult, K., Kleywegt, G.J., Patkar, S., Waagen, V., Anthonsen, T., Jones, T.A., 1995. Crystallographic and molecular-modeling studies of lipase B from Candida antarctica reveal a stereospecificity pocket for secondary alcohols. Biochemistry 34 (51), 16838–16851.

Van Der Spoel, D., Lindahl, E., Hess, B., Groenhof, G., Mark, A.E., Berendsen, H.J.C., 2005. GROMACS: fast, flexible, and free. J. Comput. Chem. 26 (16), 1701–1718.

Wang, J., Wang, W., Kollman, P.A., Case, D.A., 2001. Antechamber, an accessory software package for molecular mechanical calculations. J. Am. Chem. Soc. 222, U403.

Warshel, A., Naray-Szabo, G., Sussman, F., Hwang, J.K., 1989. How do serine proteases really work? Biochemistry 28 (9), 3629–3637.

Yuan, Y., Yang, L., Liu, S., Yang, J., Zhang, H., Yan, J., Hu, X., 2017. Enzyme-catalyzed Michael addition for the synthesis of warfarin and its determination via fluorescence quenching of l-tryptophan. Spectrochim. Acta Mol. Biomol. Spectrosc. 176, 183–188.